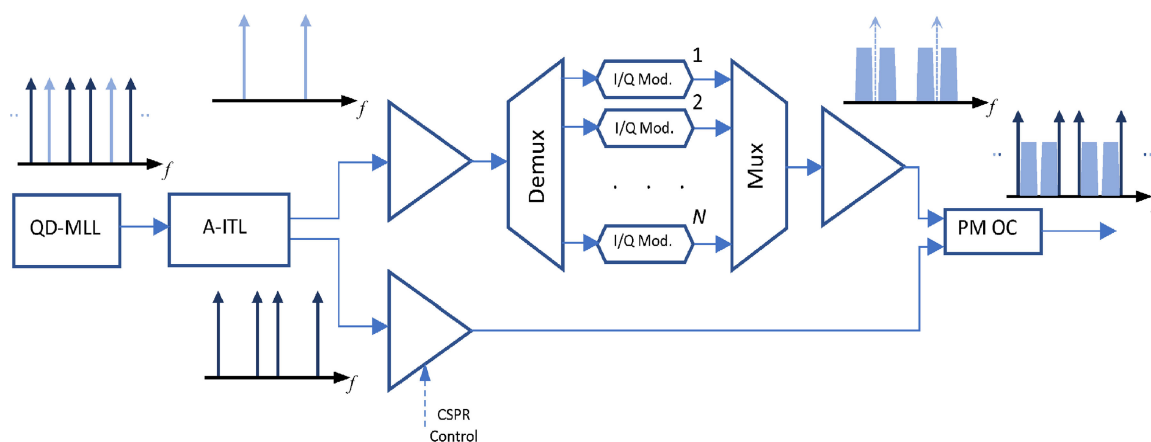# QD-MLL-Based Single-Sideband Superchannel Generation Scheme With Kramers–Kronig Direct Detection Receivers

Mustafa Al-Qadi
Govind Vedala
Maurice O'Sullivan
Chongjin Xie
Rongqing Hui

QD-MLL-Based Single-Sideband Superchannel Generation Scheme With Kramers–Kronig Direct Detection Receivers

Mustafa Al-Qadi [ORCID],[1] **Govind Vedala** [ORCID],[1] **Maurice O'Sullivan** [ORCID],[2] **Chongjin Xie** [ORCID],[3] **and Rongqing Hui**[1]

[1]M. Al-Qadi, G. Vedala, and R. Hui are with the Department of Electrical Engineering and Computer Science, University of Kansas, Lawrence, KS 66045 USA
[2]M. O'Sullivan is with the Ciena Corporation, Ottawa, ON K2K 0L1, Canada
[3]C. Xie is with the Alibaba Infrastructure Service, Alibaba Group, Sunnyvale, CA 94085 USA

Abstract: For their capability of electronic dispersion compensation, transmission systems based on direct detection of single-sideband (SSB) signals are attractive candidates as energy-efficient and cost-effective alternative solutions to intradyne digital coherent systems for interdata center and metro applications. The Kramers–Kronig (KK) receiver scheme has been shown to provide superior performance compared to other schemes in signal-to-signal beat interference (SSBI) cancelation in these direct-detection systems. In this paper, we propose a low-complexity and cost-effective scheme of generating an optical superchannel comprising multiple SSB channels, based on a single quantum-dot mode-locked laser source. The proposed system does not require additional photonic or RF components at the transmitter to generate the required SSB signal with a continuous wave (CW) carrier. It also preserves the full digital-to-analog converters' bit resolution for data modulation, in contrast to other methods based on digital generation of the CW component. Simulations of system performance with KK receiver, based on measured laser output field, show that the proposed system can achieve bit-error ratio below the hard-decision forward error correction threshold for 16-QAM Nyquist SSB signals after transmission through three amplified spans of single-mode fiber in a 240-km link. Using 8 KK channels at 23 GBaud each, the proposed scheme will be able to achieve a transmission rate of 736 Gb/s with noncoded spectral efficiency of 2.45 b/s/Hz. The impacts of carrier-to-signal power ratio, per channel launch power into the fiber, and component frequency drifting on transmission system performance are also discussed.

Index Terms: Single-sideband transmission, Kramers–Kronig receivers, Quantum-dot mode-locked lasers.

1. Introduction

The increasing demand for high data rate and high interface density optical links for metro, long reach data center interconnect (DCI) and backhaul applications has brought increased interest in developing cost-effective and energy-efficient transmission schemes to operate at $\geq$100 Gb/s. The

optical links in such applications may extend from several tens to a few hundred kilometers, making electronic dispersion compensation (EDC) an essential requirement. Direct-detection (DD) optical receivers with a single photodiode (PD) and an analog-to-digital converter (ADC) are attractive candidates for these applications for their low cost and low complexity, compared to coherent detection. To enable complex field modulation and EDC in DD systems, the signal must be transmitted in single-side band (SSB) so that the complex optical field can be translated to the electric domain at the receiver for digital processing. A known intrinsic problem of SSB DD systems is the nonlinear signal-to-signal beat interference (SSBI) noise formed at the output of the PD due to the square-law optical detection. Several techniques have been proposed to eliminate (or reduce) the effect of SSBI through receiver DSP, including the single-stage linearization filter [1], the two-stage linearization filter [2], the SSBI estimation and cancellation scheme [3], the iterative linearization method [4], and the Kramers–Kronig (KK) field reconstruction algorithm [5]. Among all these techniques, the KK algorithm has been shown by experimental comparison to provide the best receiver performance [6], making it an attractive candidate for practical SSB DD systems.

Like all other SSB self-coherent schemes, the KK scheme requires a continuous wave (CW) optical signal component to be available at one side of the information-bearing SSB signal spectrum. At the receiver, this CW component mixes with the signal sideband at the PD for the optical-to-electrical downconversion of the SSB-modulated optical signal. This CW tone can be added either at the receiver side or at the transmitter side, and the ratio of this CW power to the SSB signal power must be sufficient to satisfy the minimum phase condition required for linear reconstruction of the complex envelope of the SSB optical signal [5]. The first option is equivalent to a coherent optical receiver as a tunable laser source has to be available at the receiver which makes the hardware more complicated [7]. In comparison, generating the CW tone at the transmitter side is more practical for a simpler receiver structure. There are different techniques used to generate the CW tone at the transmitter, and each has its own intrinsic advantages and disadvantages. The CW component can be generated by biasing an electro-optic I/Q modulator above the null point and driving its inputs with the I and Q components of an SSB signal generated by digital subcarrier modulation (SCM) of the baseband data [6], [8]. In this case, the maximum optical SSB signal bandwidth is equal to the analog bandwidth B of the digital-to-analog converters (DACs) and the I/Q modulator. For the same DAC and modulator bandwidth B, the optical signal bandwidth can be doubled by utilizing carrier-suppressed complex double-sideband modulation. The CW tone can then be added at either side of the spectrum, either digitally, known as the digital virtual carrier [9], or in the analog domain by adding an RF local oscillator signal directly to the optical I/Q modulator driving signals [10], [11]. For these two bandwidth-efficient carrier insertion techniques, the first method has the disadvantage of reduced DAC resolution available for data signals by at least 50% because of the increased dynamic range of the signal (by a factor of ≥ 2) to achieve the minimum phase condition, which affects system's performance for high-order modulation formats, and hence limits system spectral efficiency [12]. The second method adds complexity to the system as an additional RF LO and wideband and sharp analog diplexers would be required to combine signals from LO and DACs without imposing significant power losses. In comparison, directly inserting a CW optical tone after the modulator may provide a better solution as it allows full utilization of the analog bandwidth of DACs and optical modulator and preserves the full bit resolution of the DACs for the information-bearing signals. Nonetheless, generating an independent CW optical tone with a precise frequency shift from the modulated optical signal will require another optical frequency-locked laser source. Otherwise, carrier-suppressed single sideband optical modulation can be used to generate a frequency-shifted optical carrier to be added to the modulated SSB signal through an optical coupler [11], [13]. This added complexity to the transmitter can be significant when multiple wavelength channels are used for wavelength division multiplexing (WDM), which is the practical case in the intended applications of metro and DCI networks.

In this paper, we propose a simple and energy-efficient scheme of generating multiple SSB signals in a superchannel configuration [14] based on a single quantum-dot mode-locked laser (QD-MLL) optical comb source and dual SCM of SSB channels. Unlike the methods mentioned above, in our proposed scheme, no additional optical or RF components are needed for the generation of the CW

tones. The dual SSB channel modulation allows for ~93% utilization of the DACs and I/Q modulator analog bandwidth for high baud rate systems (~20G Baud) and does not reduce the available DAC bit resolution for data modulation. Individual spectral lines from a QD-MLL comb source usually exhibit higher intensity and phase noises compared to single-wavelength sources used in communication applications, like distributed-feedback (DFB) lasers. Typical spectral linewidth of a QD-MLL source may vary from a few to tens of MHz [15], [16]. However, our proposed scheme utilizes the mutual coherence between adjacent spectral lines of a QD-MLL, which usually has very low differential phase noise equivalent to a linewidth of only a few tens to a few hundred kHz [16], [17]. This will reduce the receiver penalty due to laser phase noise compared to typical DFB lasers. Equivalent results can only be obtained from high-quality and relatively expensive external cavity lasers (ECLs) if the CW component is to be added from a separate laser source. System performance simulations, based on experimentally recorded complex optical field of QD-MLL, show that even in the presence of relatively high-intensity noise, the proposed system performs well below the hard-decision forward error correction (HD-FEC) threshold bit-error ratio (BER) with 16-QAM modulation for up to 240 km of standard single-mode fiber (SSMF). This makes this system an attractive solution for long-reach DCI and metro applications.

The rest of the paper is organized as follows: Section 2 provides an overview of the KK scheme, the impacts of laser phase noise and intensity noise, and presents the proposed superchannel generation scheme. Section 3 presents the details of the experimental setup and the results of QD-MLL characterization. Results of system performance analysis based on semi-numerical simulations are presented in Section 4, and Section 5 provides the conclusions.

2. SSB-Modulated Superchannel Generation

2.1 The Kramers–Kronig Self-Coherent Scheme

The KK field reconstruction algorithm is based on an essential condition of minimum phase, where the phase of an optical signal satisfying this condition can be recovered from the detected intensity [5]. Ideally, in the absence of phase noise and intensity noise, the complex envelope of the optical signal at the PD can be expressed as

$$E(t) = E_c + S(t) \exp(j\pi Bt) \tag{1}$$

and the photocurrent generated at the output of the PD, assuming a unit responsivity, is then given by

$$i(t) = |E(t)|^2 = E_c^2 + |S(t)\exp(j\pi Bt)|^2 + E_c^* \cdot S(t)\exp(j\pi Bt) + E_c \cdot S^*(t)\exp(-j\pi Bt) \tag{2}$$

where E_c is a CW carrier component, $S(t)$ is the QAM-modulated signal with total bandwidth B, and x^* represents the complex conjugate of x. $\exp(j\pi Bt)$ in (1) indicates that $S(t)$ is frequency-shifted from the carrier tone E_c by $B/2$ Hz, or equivalently, the carrier component E_c is sitting at the edge of the spectrum of $S(t)$. On the right-hand side of (2), the first term is a constant DC term, the second term represents SSBI, and the third term is the useful signal-carrier beat term containing $S(t)$. The last term is the complex conjugate of the useful signal on the opposite side of the spectrum as $i(t)$ is real. The carrier-to-signal power ratio (CSPR) of $E(t)$ in (1) is defined as $CSPR = E_c^2/\langle|S(t)|^2\rangle$, which must be high enough to satisfy the minimum phase condition required for the KK field reconstruction [5]. $\langle\cdot\rangle$ denotes time averaging.

With the KK algorithm, the reconstructed complex field signal can be obtained by

$$E_{rec}(t) = \sqrt{i(t)}\exp[j \cdot \phi_E(t)], \ \ \phi_E(t) = \mathcal{H}\left\{\log\left(\sqrt{i(t)}\right)\right\} \tag{3}$$

where $\mathcal{H}\{\cdot\}$ represents the Hilbert Transform. This reconstructed signal can be expressed as $E_{rec}(t) = E_{DC} + S_{rec}(t)\exp(j\pi Bt)$, where E_{DC} is a DC component. The baseband complex data signal $S_{rec}(t)$ can be recovered by subcarrier demodulation as

$$S_{rec}(t) = \{E_{rec}(t) - E_{DC}\} \cdot \exp(-j\pi Bt) \tag{4}$$

where E_{DC} can be practically estimated for the real and imaginary components in DSP as the mean value of the corresponding components of $E_{rec}(t)$ over a sufficient number of samples.

To include the effects of phase and intensity noises from laser source(s), (1) can be rewritten as

$$E(t) = [1 + n_c(t)] E_c e^{j\phi_c(t)} + [1 + n_m(t)] S(t) \, e^{j\phi_m(t)} e^{j\pi B t} \tag{5}$$

where $n_c(t)$ and $n_m(t)$ are zero-mean random processes with variances determined by the relative-intensity noise (RIN) of the CW carrier and the signal sideband, respectively, and $\phi_c(t)$ and $\phi_m(t)$ are their phase noise components. In this case, the carrier-signal beat term [third term in (2)] can be expressed as

$$[1 + n_c(t)] E_c e^{-j\phi_c(t)} \cdot [1 + n_m(t)] S(t) \, e^{j\phi_m(t)} e^{j\pi B t}$$
$$\approx E_c S(t) e^{j[\phi_m(t) - \phi_c(t) + \pi B t]} + [n_c(t) + n_m(t)] E_c S(t) e^{j[\phi_m(t) - \phi_c(t) + \pi B t]}. \tag{6}$$

Following the KK reconstruction procedure in (3) and (4), the recovered baseband signal can be expressed as

$$S_{rec}(t) = S(t) e^{j[\phi_m(t) - \phi_c(t)]} + [n_c(t) + n_m(t)] S(t) e^{j[\phi_m(t) - \phi_c(t)]} + n'_c(t) e^{j\phi'_c(t)} \tag{7}$$

where the first term shows that the effective phase noise in the received signal is the *differential phase noise* between the CW tone and the signal sideband $[\phi_m(t) - \phi_c(t)]$, and the second term represents the effects of carriers' intensity noises on the received signal. The third term represents the noise imposed on the received signal through the imperfect KK field reconstruction. This is because the first term of $i(t)$ in (2) is no longer a simple DC term; instead, it includes a noise component that will result in both phase, $n'_c(t)$, and intensity, $\phi'_c(t)$, fluctuations affecting the baseband constellation points after KK field reconstruction. It is evident from (3) and (6) that the noise parameters n'_c and ϕ'_c will have variances proportional to the variance of $n_c(t)$. The second term in (7) shows that the RINs of the CW tone and the signal sideband have equal contributions to transmission performance degradation. However, the RIN of the CW tone ($n_c(t)$) usually has stronger impact in the transmission performance than that of the optical carrier used for SSB modulation ($n_m(t)$) [see (6)]. This is a consequence of using high CSPR (which is usually ≥ 6 dB) to satisfy the minimum phase condition for conventional QAM signals. The analytical model presented above is derived for the back-to-back configuration with a purpose to show the impact of laser noises on the quality of the recovered signal with the KK detection. As the proposed system is based on QD-MLLs, which are known to have higher phase and intensity noises compared to typical ECL and DFB lasers, the impact of laser phase noise and intensity noise is the main focus of this section. A general analytical model for KK systems including the effects of phase-to-amplitude noise conversion through fiber chromatic dispersion and equalization-enhanced phase noise can be found in [18]. Nonetheless, noise contributions from these effects can also be mapped into the general noise term (third term) in (7) in the model presented here.

2.2 The Proposed SSB Superchannel Generation Scheme

The schematic diagram of the proposed superchannel transmitter based on QD-MLL as the light source is shown in Fig. 1. A QD-MLL generates a large number of equally spaced spectral lines, known as a frequency comb, with a free-spectral range (FSR) ΔF. The QD-MLL is selected as the comb source for this system for its higher energy efficiency compared to four-wave-mixing-based ring resonator comb sources [19] and its practical frequency spacing compared to passively mode-locked fiber lasers [20]. In the proposed system, the output of QD-MLL is first fed to an optical asymmetric interleaver (A-ITL) [21]–[23] with an FSR of 3 ΔF and 30%/70% frequency band assignments for the odd and even channels as illustrated in Fig. 2, where $\Delta F = 25$ GHz is assumed. The "30% port" of the interleaver selects spectral lines spaced by 3 ΔF, and the "70% port" selects pairs of adjacent spectral lines spaced by ΔF. The spacing between the closest lines of two neighboring pairs is 2 ΔF. As shown in the insets of Fig. 1, the 3 ΔF-spaced line pairs are amplified and demultiplexed for data modulation. Every demultiplexed carrier is modulated
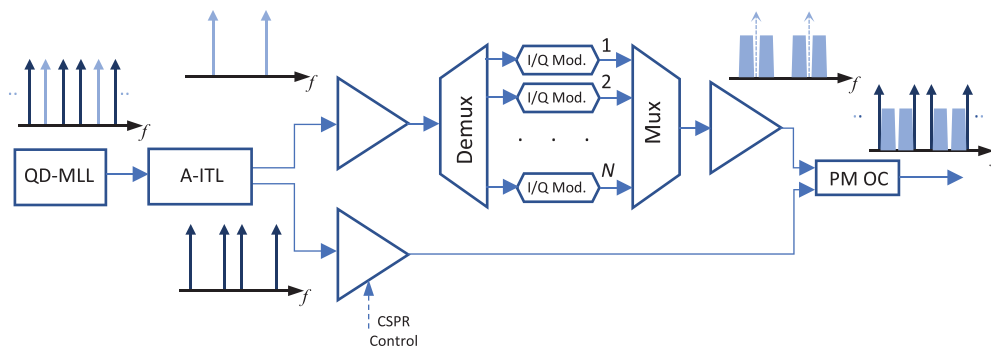
Fig. 1. Schematic of the proposed SSB superchannel transmitter. A-ITL: asymmetric interleaver. PM OC: polarization-maintaining optical combiner. Amp: optical amplifier.
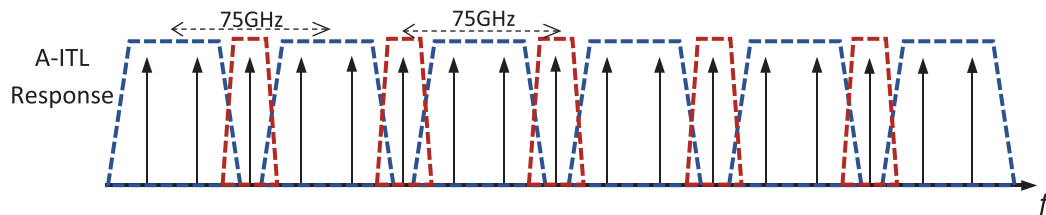

Fig. 2. Ideal transfer function of the 37.5–75 GHz asymmetric (30%/70%) deinterleaver used to separate comb lines.

with two Nyquist SCM channels, one on each side of the optical carrier, through an optical I/Q modulator. These two subcarrier-modulated sidebands can carry independent Nyquist QAM signals multiplexed in the transmitter DSP, so that the I and Q RF signals driving each modulator contain data of two independent SCM channels. The modulator must be biased at the null point so that the optical carrier is suppressed, as shown in the inset of Fig. 1, where the suppressed carriers after optical modulation are shown as dashed arrows for the purpose of illustration. After multiplexing and amplifying the modulated channels, the CW pairs from the "70% port" output of the A-ITL are amplified and recombined with the modulated signals. The CSPR can be simultaneously set for all channels by controlling the gain of the optical amplifier for the CW tones. It is of high importance to ensure that the modulated optical signals and the CW tones are co-polarized when they combine. One way to ensure this is to use polarization maintaining optical connections and components in the transmitter. The optical amplifiers in this transmitter can be in the form of semiconductor optical amplifiers (SOAs). With the recent advances in photonics integration, this transmitter structure may be realized in an integrated planar lightwave circuit (PLC), allowing for small footprint and low cost [24]–[27].

The asymmetric channel configuration of the resulting superchannel uses N I/Q modulators to support $2N$ independent data channels, and the frequency spacing between adjacent channel pairs is $\triangle F$. This provides relaxed requirements on the optical filters used to select individual channels at the receiver. A similar channel plan was proposed in [28], where, in contrast to our proposed system, each WDM channel was generated individually using a dedicated laser source and an I/Q modulator. For a conventional WDM frequency grid with equal channel spacing filled by the SSB-modulated signal on one side of each CW carrier, spectral components of adjacent channel can create significant crosstalk if the optical filter is not sharp enough. For the superchannel frequency arrangement in the proposed system in Fig. 1, however, spectral guard band ($\triangle F$) reserved between each pair of channels (25 GHz in this example) helps relaxing the spectral selectivity requirements of receiver optical filters. Crosstalk from the nearest channel [see Fig. 5(a)] only creates high-frequency components ($>\triangle F$) when mixing with the CW carrier, which does not affect the SSB
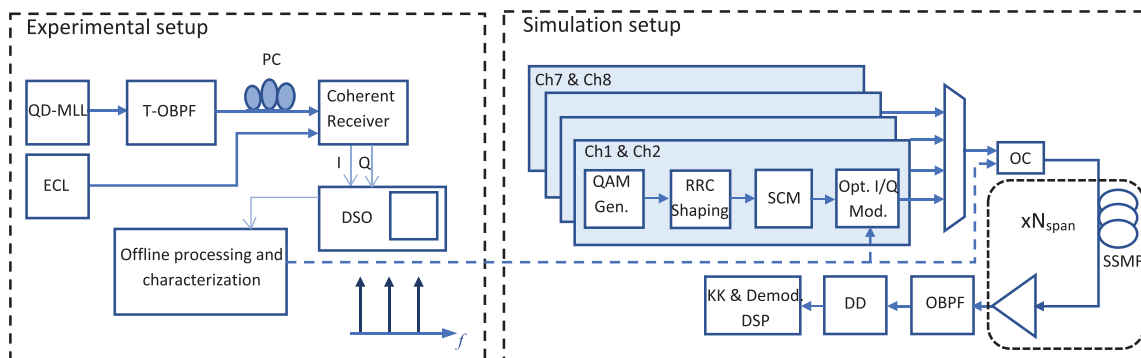
Fig. 3. Experimental and simulation setup schematics. T-OBPF: tunable optical bandpass filter. PC: polarization control. ECL: external cavity laser. DSO: digital storage oscilloscope. RRC: root-raised cosine. SCM: subcarrier modulation. OC: optical combiner. DD: direct detection.

condition. Therefore, only a very small guard band can be sufficient between the two channels in a pair to avoid their interference, which compensates for the relatively wide gap ΔF between channel pairs and results in an overall superchannel uncoded spectral efficiency of $\frac{2}{3}\eta\log_2(M)$ b/s/Hz, where η is the system baud to ΔF ratio, and M is the QAM modulation order. Furthermore, with this channel allocation, grid channel selection at the receiver may be done by using deinterleavers with offset center frequencies and equal FSRs followed by conventional low-cost arrayed waveguide grating (AWG) filters, as was proposed in [11], [28].

3. Experimental Setup and QD-MLL Characterization

To demonstrate the practicality of adopting the QD-MLL comb sources in the transmission of an SSB superchannel in the proposed transmitter scheme for KK reception, we first characterize the phase and intensity noise properties of a single-section InAs/InP QD-MLL with 25 GHz repetition frequency (FSR). The driving current of the laser was set to 400 mA at an operating temperature of 19 °C. This MLL operates in the lower half of the C-band with a 3-dB spectral bandwidth of 1.35 THz in the wavelength range of 1532.0–1542.5 nm, consisting of 54 equally spaced spectral lines with 25 GHz channel spacing. The optical spectrum of the laser output is shown in Fig. 4(a), which was measured by an optical spectrum analyzer with 0.01 nm resolution bandwidth. To characterize the phase and intensity noises of individual spectral lines, a coherent I/Q receiver was employed with a tunable ECL as the LO, which has a full-width at half-maximum (FWHM) linewidth of <50 kHz. A 1-nm tunable optical bandpass filter was used to select a set of comb lines with the state of polarization aligned to that of the LO through a polarization controller to maximize the mixing efficiency. The complex beat tones between the LO and the nearest two comb lines of the QD-MLL were recorded using a digital storage oscilloscope operating at 50 GS/s with 23 GHz of analog bandwidth. The measured electrical SNR after sampling was 57 dB in a resolution bandwidth of 50 kHz. The recorded waveforms were processed offline for evaluating the phase and intensity noises of the comb lines. Optical transmission system performance was then evaluated numerically using the measured complex field of the MLL comb lines as the optical sources. Schematic diagrams of the experimental and simulation setups of this work are shown in Fig. 3.

In the process of characterizing phase noise and RIN of QD-MLL comb lines, the recorded coherent detection waveforms were used, which represent a downshifted version of the complex optical field of QD-MLL spectral lines into the RF domain. An ideal BPF with 2 GHz bandwidth was applied to select the spectral line under consideration and limit the broadband receiver noise. For phase noise measurement, the linewidth of each selected comb line was calculated from the variance of the phase difference between field samples spaced at $\tau = 10$ ns as $\delta f = \sigma^2/(2\pi\tau)$, where σ^2 is the variance of the phase difference sequence. As shown in Fig. 4(a), the linewidths were
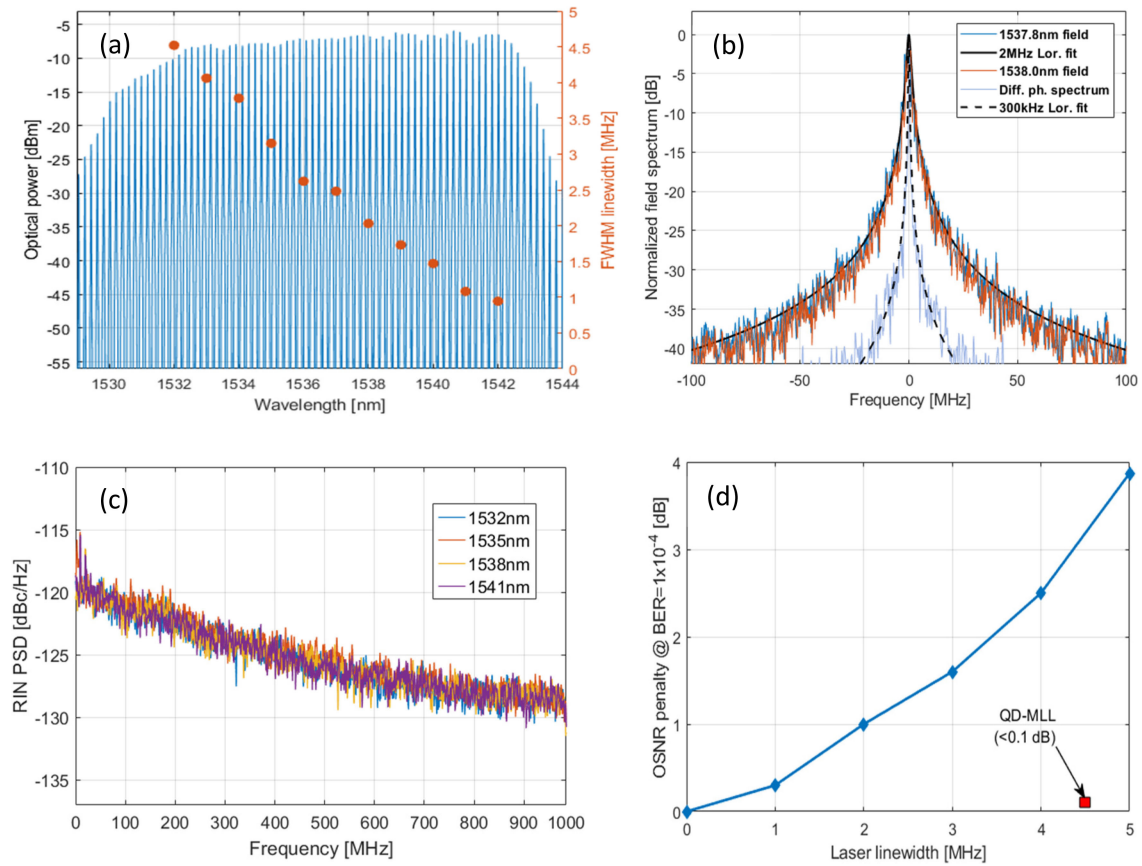
Fig. 4. (a) Optical spectrum of the 25 GHz QD-MLL and linewidth of some selected comb lines. (b) Field spectra of two adjacent comb lines from the middle of the comb band with a Lorentzian fitting corresponding to their average linewidth, and their differential phase spectrum. (c) RIN spectral profiles of some selected wavelengths. (d) Simulated OSNR penalty from laser phase noise in 23 GBaud 16-QAM KK transmission using the QD-MLL measured phase noise waveforms, compared to using independent lasers with different linewidths.

found to vary between 0.9 and 4.5 MHz within the spectral window of the QD-MLL depending on the wavelength, similar to what was found in [16], [17] for the same type of MLLs. The spectra of two adjacent spectral lines are shown in Fig. 4(b) which can be best fitted by the Lorentzian function with 2 MHz FWHM linewidth. Also shown in the same figure is the spectrum of the differential phase between these two comb lines, which was obtained by multiplying one of the tones with the complex conjugate of the other in the time domain. The differential phase was found to have a variance equivalent to 300 kHz of FWHM Lorentzian linewidth. Note that the accuracy of determining the differential phase noise is not affected by the linewidth of the LO as it is common for both spectral lines. Fig. 4(c) shows the measured RIN spectral profiles of four comb lines, obtained by extracting the perturbations in the magnitude of the field envelope through time averaging and mean subtraction. Unlike the case of the phase noise, comb lines of different wavelengths have very similar RIN characteristics with a higher spectral density at the low-frequency region extending to 1 GHz. No correlation was found between intensity noises of adjacent comb lines.

The small differential phase noise between adjacent comb lines is a key feature of QD-MLL sources that makes them suitable for the proposed scheme in this work. As was shown in Section 2.1, the effective phase noise in KK transmission is determined by the phase difference between the modulated signal sidebands and the CW tone. Therefore, despite the relatively broad linewidths of individual spectral lines, QD-MLL sources are expected to perform well in this trans-

mission scheme. To verify this property, the measured optical fields of two adjacent comb lines (1532 and 1532.2 nm), both with linewidths of approximately 4.5 MHz, were used in the simulation to generate one SSB channel of 23 GBaud 16-QAM signal together with the required CW tone for KK detection in a back-to-back configuration. Fig. 4(d) shows the optical signal-to-noise ratio (OSNR) penalty calculated at the BER level of 10^{-4} after noise loading compared to the ideal case in the absence of phase noise. Details of the simulation procedure are provided in the next section. As shown in Fig. 4(d), the QD-MLL exhibits a very small penalty ($<$0.1 dB) compared to the case of using independent lasers. In this simulation, the phase noise in the case of independent lasers was generated as a Weiner process with variance of $\sigma^2 = 2\pi\delta f\,T_s$, where T_s is the sampling (symbol) period. Equal linewidths for the modulated signal and the CW tone were assumed for every point in Fig. 4(d). Systems of relatively low baud rates are more susceptible to laser phase noise; and maintaining a low linewidth-symbol period product ($\delta f \times T_s$) is important to limit phase noise penalty [29]. Lasers with very low phase noise are usually of high cost, which might exceed the feasible system design budget for applications such as access and mobile backhauling networks. It is worth mentioning that the phase-noise-induced system penalty after fiber transmission is not only limited to the penalties presented in Fig. 4(d), but will also include SNR penalties from phase-to-amplitude conversion and equalization-enhanced effects [18], which will inherently be included in the numerical simulations presented in Section 4.

4. System Performance Semi-Numerical Simulation Results

In the QD-MLL characterization, the captured complex waveforms from the coherent I/Q receiver preserve the full information of the phase and intensity noises. As the complex optical fields of adjacent optical spectral lines are captured simultaneously, their phase relation is also captured. Therefore, they can be used for accurate transmission performance evaluation through computer simulation with practical system parameters and numerical models implemented in MATLAB. The block diagram of simulation setup is shown in Fig. 3. Eight independent 16-QAM data channels were generated at 23 GBaud from random binary data sets, up-sampled and Nyquist-pulse-shaped by a root-raised cosine (RRC) filter with a roll-off factor of 0.05. The binary data were differentially mapped into the 16-QAM constellation points, where the first two bits in a nibble were used to differentially determine the quadrant with Gray coding, and the other two bits were used to determine the symbol in that assigned quadrant [29]. Next, four SCM channel pairs were formed, and each pair consists of two data channels of $\sim$23 GHz bandwidth, and they are mixed with subcarriers at $\pm$13.25 GHz, so that the spacing between them is $\sim$3.5 GHz. The four pairs of data channels were complex I/Q modulated into optical domain with different quasi-optical carrier frequencies spaced by 75 GHz ($3\Delta F$) as shown in Fig. 5(a). The DACs were assumed to have a frequency-independent resolution of 8 bits throughout the simulation steps. The captured complex optical field containing two adjacent comb lines of the QD-MLL were demultiplexed, normalized, and resampled to match the simulation sampling rate. One of them was used to carry Ch5 and Ch6, and the other one on the left edge of Ch5 is used as the CW tone for KK detection of Ch5. Optical carriers of all other channels, as crosstalk channels, are ideal without noise. This results in a 250 MHz of guard band between the Nyquist channel and its corresponding CW tone in the optical domain, and a value of $\eta = 0.92$. The overall superchannel noncoded spectral efficiency is 2.45 b/s/Hz (8 channels $\times$ 23 GBaud $\times$ 4 bits/300 GHz $= \frac{2}{3}\eta\log_2(M)$, $\eta = 0.92$, $M = 16$) with total superchannel noncoded (line) transmission rate of 736 Gb/s.

For KK detection, the receiver simulation uses a third-order super-Gaussian bandpass filter with 35 GHz bandwidth, which is centered at 10.35 GHz (0.45 $\times$ baud) from the CW tone of Ch5 [shown in purple dashed line in Fig. 5(a)] to represent a WDM demultiplexer. This is followed by an ideal PD [30] and an ADC of 8-bit resolution. After the ADC, the KK field reconstruction (3)was implemented at a sampling rate of 6 Sam/Sym, followed by downsampling to 2 Sam/Sym, DC removal, and frequency downconversion (4). EDC is then applied, in case of fiber transmission, and the signal is sent to demodulation DSP. The demodulation DSP comprises a matched RRC filter followed by a feed-forward blind equalizer for sample retiming and signal quality improvement,
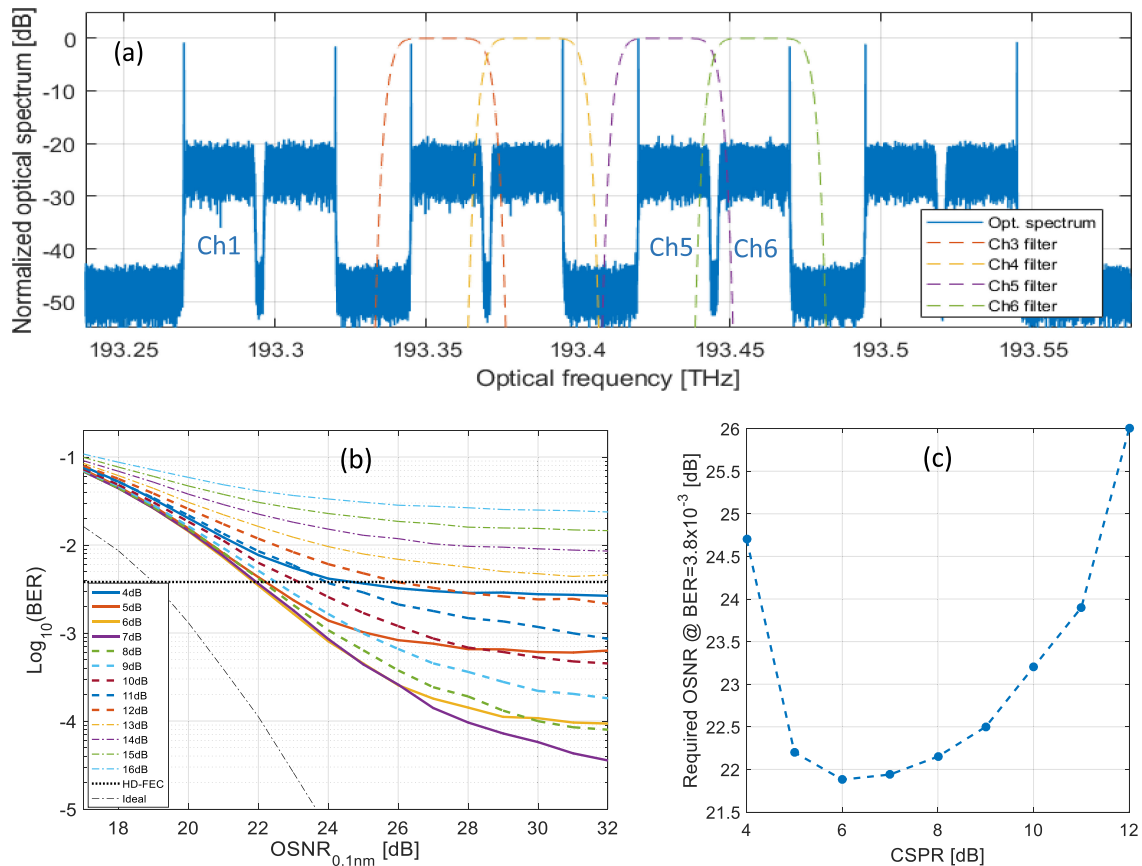
Fig. 5. (a) Spectrum of the generated optical superchannel in simulation. (b) Back-to-back BER performance versus OSNR for different values of CSPR. (c) Required OSNR at the 7% HD-FEC threshold (3.8×10^{-3}) for different CSPR values. Dotted-dashed line shown in (b) represents system performance with ideal optical and electrical components at 7-dB CSPR.

carrier phase recovery based on constellation partitioning and the fourth power algorithm [31], and a hard-decision symbol-to-bit differential demapping.

System performance was first tested in back-to-back configuration with noise loading. The BER was calculated by error counting for different values of CSPR by changing the power of added noise to vary the OSNR. At least 2 million symbols (8 million bits) were transmitted for every BER point for all the results presented in this work. The OSNR is defined here as the power ratio of the SSB-modulated signal without the CW tone to the power of ASE noise in a 0.1-nm bandwidth. Fig. 5(b) shows that with CSPR of <6 dB, the transceiver performance is degraded with BER floors at high OSNR values because the minimum phase condition is not satisfied. On the other hand, by increasing the CSPR beyond 8 dB, the performance also deteriorates as shown in dashed-curves in Fig. 5(b). This is attributed to the strong beating between the CW tone and the ASE noise at the opposite side of the carrier, which violates the SSB condition. With higher CSPR values ≥13 dB, the BER performance could not achieve the 7% HD-FEC conventional threshold of 3.8×10^{-3} even for high OSNR values of up to 32 dB [shown in dashed-dotted curves in Fig. 5(b)]. Comparing the BER performances corresponding to CSPR of 6 and 7 dB, one finds that they exhibit optimality in different regions of OSNR values. This would suggest that CSPR should be optimized for the specific OSNR of the system to achieve the optimum performance. However, the difference in BERs is very small for a wide range of OSNRs (22–28 dB) achieving BER performance above the FEC threshold; and choosing a fixed CSPR value at the system design stage would achieve acceptable
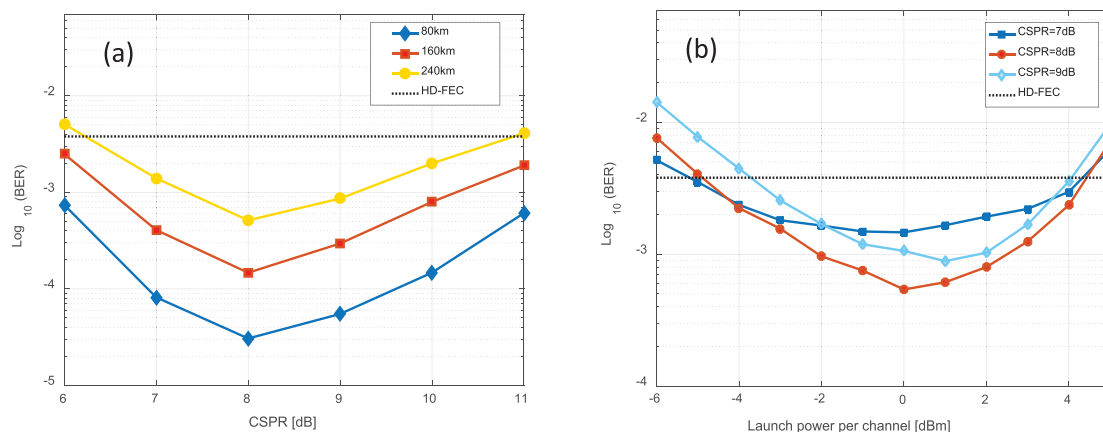
Fig. 6. (a) BER versus CSPR at optimum launch power values for different link lengths. (b) BER versus launch optical power per channel for 3 spans (240 km) at different values of CSPR.

performance without the complexity of required Rx-to-Tx feedback control loop. Fig. 5(c) shows the required OSNR at the HD-FEC threshold for different values of CSPR. The optimum CSPR value was found to be at 6 dB. All CSPR values below 6 dB violate the minimum phase condition. CSPR values of higher than 6 dB will introduce linear degradation due to the high power of CW tone which mixes with the ASE noise on both sides of the spectrum around the CW tone. It is also clear that the required OSNR varies only for less than 0.5 dB for CSPRs spanning the range from 5 to 8 dB.

To simulate system performance with fiber transmission, the superchannel was sent through a fiber link consisting of 1, 2, or 3 spans, each of 80 km of standard single-mode fiber (SSMF) with a dispersion parameter $D = 17$ ps/nm/km, a nonlinear parameter $\gamma = 1.2$ W^{-1} km^{-1}, and a loss factor of 0.2 dB/km. Each fiber span is followed by an erbium-doped fiber amplifier with 5 dB noise figure, and the total single span loss was assumed to be of 20 dB to account for splice and connector losses in an actual fiber link. The symmetric split-step Fourier method was used to simulate signal propagation, so that both dispersion and Kerr nonlinearity impairments are included in the results presented here. Fig. 6(a) shows the BER versus the CSPR values for different number of spans in the fiber link. These BER values were calculated at the optimum launch power per channel including both the signal sideband and CW tone. The optimum CSPR value is clearly different from what was found in the back-to-back configuration. In comparison, one finds that this optimum CSPR value is about ~2 dB less than what is found in other works (like in [9] or [32], for instance), which is attributed to the high RIN in the CW tone used in our work, as was discussed in Section 2.1. Nonetheless, the system still achieves BER values below the HD-FEC threshold for the 240 km link over >4 dB window of CSPRs. Fig. 6(b) shows the dependence of system performance on the launched optical power per WDM channel for the 240 km link. The optimum launched power is found to increase with the increase of the CSPR value. For the optimum CSPR of 8 dB, the optimum power was found to be at 0 dBm. For all three CSPR values used in Fig. 6(b), varying the launch power to ±4 dB from the optimum value still keeps the BER value below the HD-FEC threshold.

The KK algorithm is known to require an oversampling ratio higher than the typical 2 Sam/Sym due to the broadening of the spectrum caused by the nonlinear logarithm operation, which increases DSP complexity and energy consumption. Some alternative schemes of implementing the KK algorithm were proposed to avoid the logarithm operation, but they still require repetitive or additional operations that add their own computational complexities [5], [33]. This oversampling requirement is of high importance in energy-sensitive applications such as DCI. Fig. 7(a) shows the dependence of receiver BER on oversampling used in the implementation of the KK algorithm in our simulation. The results indicate that an oversampling ratio of 4 Sam/Sym can still achieve acceptable performance with a small BER penalty compared to 6 Sam/Sym for the proposed system with QD-MLL as
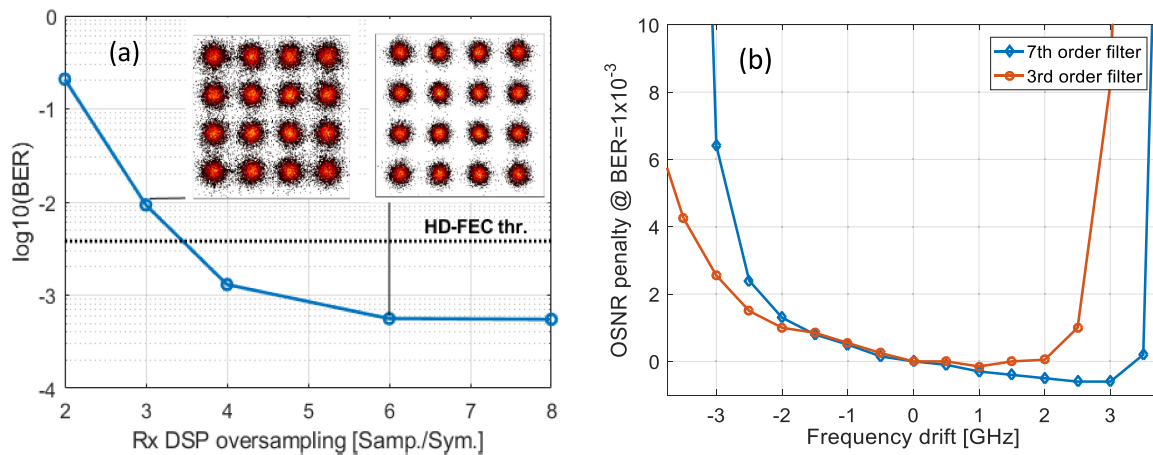
Fig. 7. (a) BER versus KK oversampling ratio for 240 km with optimum CSPR (8 dB) and launch power (0 dBm). (b) OSNR penalty (dB) at BER $= 10^{-3}$ versus receiver optical filter frequency drift for third- and seventh-order super-Gaussian filter response in B2B configuration with noise loading. EVM values of constellations in insets of (a) are 10.8% and 14.9% for 6 Sam/Sym and 3 Sam/Sym, respectively.

the optical source. The selection of the KK algorithm implementation scheme in system design will depend on the symbol rate, energy consumption constraints, and the power/OSNR budget of the application.

Finally, the sensitivity to the center frequency drift of the optical filter at the receiver is investigated by changing the center frequency of the 35 GHz super-Gaussian filter with the orders of 3 and 7. The OSNR penalties for BER $= 10^{-3}$ are shown in Fig. 7(b). The asymmetry of the penalty with respect to the direction of filter drifting can be explained as follows. Consider Ch. 5 in Fig. 5(a), when the bandpass filter shifts to a higher frequency, less amount of ASE noise on the left side of the CW tone is selected, which improves the performance as long as the drift is small enough and the CW tone is not attenuated. Once the positive drift significantly attenuates the CW tone, system performance degrades rapidly. On the other hand, for the filter drifting to the lower frequency, the cutoff of the continuous signal spectrum is gradual, so is the performance degradation. It is also shown in Fig. 7(b) that the quality (edge sharpness) of the filter does not improve the performance tolerance to negative frequency drift if the filter is centered at the same frequency relative to the data spectrum. Therefore, the choice of filter center frequency should be optimized for different filter transfer functions and drifting tolerances. It is worth mentioning that as the frequency drifting is relative between the filter and the laser, the penalty caused by QD-MLL frequency drift is also predicted as in Fig. 7(b). In general, frequency drifts of QD-MLL affect all comb lines equally with little change in the frequency spacing. For instance, in the QD-MLL used in our experimental work, the differential frequency drift between adjacent comb lines was only in the order of a few MHz for the common-mode frequency drift of multiple GHz due to temperature changes. This small differential frequency drift can be easily eliminated in receiver DSP by a frequency offset compensation algorithm.

5. Conclusion

In this paper, we have proposed a low-complexity and cost-effective scheme for generating a superchannel of SSB modulation based on a single QD-MLL optical source. By utilizing the mutual coherence between adjacent comb lines, the proposed system has been shown through experimental measurement of a QD-MLL and numerical simulations to exhibit good system performance, despite the relatively high individual linewidths and RIN of QD-MLL comb lines. The system was shown to perform below the HD-FEC threshold for up to three spans of SSMF extending up to

240 km with 16-QAM Nyquist-SCM channels, achieving an overall superchannel line spectral efficiency of 2.45 b/s/Hz. Compared to conventional systems of generating WDM SSB channels based on multiple laser sources, our proposed system simultaneously provides optimum utilization of DAC bit resolution and analog bandwidth of DAC and optical I/Q modulators without the need for additional RF or optical components to achieve this result. Furthermore, the adoption of QD-MLL together with the dual channel modulation technique in the proposed system reduces the cost and footprint of the system by using half the number of DACs and I/Q modulators compared to those required in conventional multichannel generation systems, and hence provides higher energy efficiency. With the recent advances of integrated photonics and electro-optic modulators, the transmitter of the proposed system is suitable for integration on PLC platforms.

Acknowledgment

References

[1] S. Randel, D. Pilori, S. Chandrasekhar, G. Raybon, and P. Winzer, "100-Gb/s discrete-multitone transmission over 80-km SSMF using single-sideband modulation with novel interference-cancellation scheme," in *Proc. Eur. Conf. Opt. Commun.*, 2015, Paper Mo.4.5.2.

[2] Z. Li *et al.*, "Two-stage linearization filter for direct-detection subcarrier modulation," *IEEE Photon. Technol. Lett.*, vol. 28, no. 24, pp. 2838–2841, Dec. 2016.

[3] Z. Li *et al.*, "Reach enhancement for WDM direct-detection subcarrier modulation using low-complexity two-stage signal-signal beat interference cancellation," in *Proc. Eur. Conf. Opt. Commun.*, 2016, Paper M.2.B.1.

[4] K. Zou, Y. Zhu, F. Zhang, and Z. Chen, "Spectrally efficient terabit optical transmission with Nyquist 64-QAM half-cycle subcarrier modulation and direct-detection," *Opt. Lett.*, vol. 41, no. 12, pp. 2767–2770, 2016.

[5] A. Mecozzi, C. Antonelli, and M. Shtaif, "Kramers–Kronig coherent receiver," *Optica*, vol. 3, no. 11, pp. 1220–1227, 2016.

[6] Z. Li *et al.*, "SSBI mitigation and the Kramers–Kronig scheme in single-sideband direct-detection transmission with receiver-based electronic dispersion compensation," *J. Lightw. Technol.*, vol. 35, no. 10, pp. 1887–1893, May 2017.

[7] Y. Zhu *et al.*, "Single carrier 400G transmission with single-ended heterodyne detection," *IEEE Photon. Technol. Lett.*, vol. 29, no. 21, pp. 1788–1791, Nov. 2017.

[8] M. S. Erkılınç *et al.*, "Spectrally efficient WDM Nyquist pulse-shaped 16-QAM subcarrier modulation transmission with direct detection," in *J. Lightw. Technol.*, vol. 33, no. 15, pp. 3147–3155, Aug. 2015.

[9] S. T. Le *et al.*, "1.72-tb/s virtual-carrier-assisted direct-detection transmission over 200 km," *J. Lightw. Technol.*, vol. 36, no. 6, pp. 1347–1353, Mar. 2018.

[10] B. J. C. Schmidt *et al.*, "Low sample rate transmitter for direct-detection optical OFDM," in *Proc. OSA Opt. Fiber Commun. Conf. Expo./Nat. Fiber Optic Engineers Conf.*, 2009, Paper OWM4.

[11] X. Chen *et al.*, "Kramers–Kronig receivers for 100-km datacenter interconnects," *J. Lightw. Technol.*, vol. 36, no. 1, pp. 79–89, Jan. 2018.

[12] C. Laperle and M. O'Sullivan, "Advances in high-speed DACs, ADCs, and DSP for optical coherent transceivers," *J. Lightw. Technol.*, vol. 32, no. 4, pp. 629–643, Feb. 2014.

[13] X. Chen *et al.*, "218-Gb/s single-wavelength, single-polarization, single photodiode transmission over 125-km of standard single mode fiber using Kramers–Kronig detection," in *Proc. Opt. Fiber Commun. Conf.*, 2017, Paper Th5B.6.

[14] X. Liu and S. Chandrasekhar, "Superchannel for next-generation optical networks," in *Proc. Opt. Fiber Commun. Conf. OSA Technical Digest* [Online]. Optical Society of America, 2014, Paper W1H.5.

[15] M. Al-Qadi, G. Vedala, and R. Hui, "Phase noise of diode laser frequency comb and its impact in coherent communication systems," in *Proc. Conf. Lasers Electro-Opt.*, San Jose, CA, USA, 2018, pp. 1–2.

[16] K. Zanette, J. C. Cartledge, and M. O'Sullivan, "Correlation properties of the phase noise between pairs of lines in a quantum-dot optical frequency comb source," in *Proc. Opt. Fiber Commun. Conf. Exhib.*, 2017.

[17] G. Vedala, M. Al-Qadi, M. O'Sullivan, J. Cartledge, and R. Hui, "Phase noise characterization of a QD-based diode laser frequency comb," *Opt. Exp.*, vol. 25, pp. 15890–15904, 2017.

[18] S. T. Le, K. Schuh, and H. Nguyen Tan, "A closed-form expression for direct detection transmission systems with Kramers–Kronig receiver," *IEEE Photon. Technol. Lett.*, vol. 30, no. 23, pp. 2048–2051, Dec. 2018.

[19] M. A. Foster, J. S. Levy, O. Kuzucu, K. Saha, M. Lipson, and A. L. Gaeta, "Silicon-based monolithic optical frequency comb source," *Opt. Exp.*, vol. 19, pp. 14233–14239, 2011.

[20] B. R. Washburn, S. A. Diddams, N. R. Newbury, J. W. Nicholson, M. F. Yan, and C. G. Jorgensen, "Phase-locked, erbium-fiber-laser-based frequency comb in the near infrared," *Opt. Lett.*, vol. 29, pp. 250–252, 2004.

[21] S. Cao *et al.*, "Interleaver technology comparisons and applications requirements," *J. Light. Technol.*, vol. 22, no. 1, pp. 281–289, 2004.

[22] H.-W. Lu, K.-J. Wu, Y. Wei, B.-G. Zhang, and G.-W. Luo, "Study of all-fiber asymmetric interleaver based on two-stage cascaded Mach–Zehnder Interferometer," *Opt. Commun.*, vol. 285, no. 6, pp. 1118–1122, 2012.

[23] An example commercial product specifications may be found online: http://www.optoplex.com/Asymmetric_Interleaver. htm

[24] L.-W. Luo *et al.*, "High bandwidth on-chip silicon photonic interleaver," *Opt. Exp.*, vol. 18, pp. 23079–23087, 2010.

[25] M. Zhang *et al.*, "Ultra-high bandwidth integrated lithium niobate modulators with record-low V_π," in *Proc. Opt. Fiber Commun. Conf.*, 2018, Paper Th4A.5.

[26] H. Park, A. W. Fang, O. Cohen, R. Jones, M. J. Paniccia, and J. E. Bowers, "A hybrid AlGaInAs-silicon evanescent amplifier," *IEEE Photon . Technol . Lett* ., vol. 19, no. 4, pp. 230–232, Feb. 2007.

[27] K. V. Gasse, R. Wang, and G. Roelkens, "27 dB gain III–V-on-silicon semiconductor optical amplifier with >17 dBm output power," *Opt. Exp.*, vol. 27, pp. 293–302, 2019.

[28] X. Chen *et al.*, "4 × 240 Gb/s dense WDM and PDM Kramers–Kronig detection with 125-km SSMF transmission," in *Proc. 2017 Eur. Conf. Opt. Commun.*, Gothenburg, Sweden, 2017, pp. 1–3.

[29] T. Pfau, S. Hoffmann, and R. Noe, "Hardware-efficient coherent digital receiver concept with feedforward carrier recovery for M-QAM constellations," *J. Light. Technol.*, vol. 27, no. 8, pp. 989–999, Apr. 2009.

[30] X. Chen, S. Chandrasekhar, S. Olsson, A. Adamiecki, and P. Winzer, "Impact of O/E front-end frequency response on Kramers–Kronig receivers and its compensation," in *Proc. Eur. Conf. Opt. Commun.*, Rome, Italy, 2018, pp. 1–3.

[31] I. Fatadin, D. Ives, and S. J. Savory, "Carrier phase recovery for 16-QAM using QPSK partitioning and sliding window averaging," *IEEE Photon . Technol . Lett* ., vol. 26, no. 9, pp. 854–857, May 2014.

[32] Z. Li *et al.*, "Joint optimisation of resampling rate and carrier-to-signal power ratio in direct-detection Kramers–Kronig receivers," in *Proc. Eur. Conf. Opt. Commun.*, Gothenburg, Sweden, 2017, pp. 1–3.

[33] T. Bo and H. Kim, "Kramers–Kronig receiver operable without digital upsampling," *Opt. Exp.*, vol. 26, 2018, Art. no. 13810.